

Varaha: A promising sampler for obtaining gravitational wave posteriors.

Vaibhav Tiwari,¹★

¹*Institute of Gravitational Wave Astronomy, School of Physics and Astronomy, University of Birmingham, Edgbaston, Birmingham B15 2TT, UK*

Accepted XXX. Received YYY; in original form ZZZ

ABSTRACT

Nested sampling has been the workhorse for estimating parameters of compact binaries from the gravitational wave signals. It operates using a set of live points and accepts/rejects points drawn from prior such that the live point with the lowest likelihood is replaced by a point with a higher likelihood value. Each such iteration shrinks the volume enclosed by the live point of lowest likelihood by a known factor. The estimated sampling density along with the likelihood values of the new and old live points quantifies the probability mass enclosed by them. Although robust, nested sampling often discards a majority of the sampled points ($\sim 99.9\%$) at which likelihood was calculated. However, for small dimensional problems, which happens to be the case for compact binaries, the sampling density of all the sampled points can be explicitly calculated thereby removing the need to discard samples. The points' sampling density and likelihood values constitute the posterior distribution. Avoiding the wastage implies significant improvement in the sampling efficiency. In a previous method, we presented a recipe to reconstruct the live volume; the volume that encloses most of the posterior probability mass. We build on this method and present a methodology that explicitly records the sampling density of all the points. For small dimensions, the presented sampler is significantly more efficient than the canonical nested samplers and is embarrassingly parallel.

Key words: Gravitational waves - methods: data analysis

1 INTRODUCTION

Parameter estimation of compact binaries from their gravitational wave (GW) signal is essential for inferring the compact binary population, conducting tests of general relativity, or performing cosmological studies (e.g. see Farah et al. (2023); Ray et al. (2023); Adamcewicz et al. (2023); Heinzel et al. (2023); Sadiq et al. (2024); Gupta (2024); Rinaldi et al. (2024); Callister & Farr (2024); Payne et al. (2024); Magaña Hernandez & Ray (2024); Leyde et al. (2024); The LIGO-Virgo-KAGRA (LVK) Collaboration (2023) for some recent works).

Compact binary parameters are often estimated using Monte Carlo methods where the likelihood is calculated for hundreds of millions of data points drawn from the parameter space. Each likelihood calculation can take a few tens to a few thousand milliseconds (Pratten et al. 2021). In addition, multiple copies of each analysis are run to collect a sufficient number of posterior samples, and each signal is analysed several times using different waveforms and sometimes with various choices on the prior distribution (Abbott et al. 2021a,b). The overall computational load, although enormous, has been manageable.

However, with ground-based GW detectors becoming increasingly sensitive the number of observed GW signals is expected to be in the hundreds per year (Abbott et al. 2020). The total computational cost for estimating the parameters is expected to rise proportionally. Additional computational load is expected due to increased sensitivity. Improvement at lower frequencies will require the generation of longer-duration gravitational waveforms to estimate the param-

eters. Increased sensitivity will also enable the measurement of new parameters, e.g. eccentricity, which will likely require increased computation. Often, analyses need to be micromanaged for a variety of reasons, and with each analysis finishing over multiple days, the increased detection rate may pose a logistical challenge.

Significant efforts have been aimed at addressing these challenges. These efforts have focused on making approximate but fast estimations of parameters (Fairhurst et al. 2023), speeding up likelihood calculation which constitutes a major fraction of the computational load (e.g. see Morisaki & Raymond (2020); Morisaki (2021); Pathak et al. (2023); Morisaki et al. (2023); Narola et al. (2023); Morrás et al. (2023); Pathak et al. (2024); Roulet et al. (2024) for some relevant works.), and improving the sampling efficiency of the analysis using machine learning (Williams et al. 2021; Dax et al. 2021; Gabbard et al. 2022; Wong et al. 2023).

It is also possible to break the sampling problem into the observer dependent (extrinsic) parameters and observer independent (intrinsic) parameters (Pankow et al. 2015; Lange et al. 2018; Tiwari et al. 2023; Wong et al. 2023). For fixed intrinsic parameters, the likelihood for arbitrary extrinsic parameters can be obtained by applying amplitude/phase shifts to the waveform. To obtain posterior, the likelihood is first marginalised over extrinsic parameters for fixed intrinsic parameters. Following this, the intrinsic parameters are sampled using the marginalised likelihoods. The analysis incurs an additional cost for obtaining marginalised likelihoods but requires a significantly smaller number of waveform generations as the sampling over the intrinsic parameters is performed on dimensionally small parameter space.

All parameter estimation analyses benefit from improvements in sampling schemes. In this article, we present a novel sampling

★ E-mail: v.tiwari@bham.ac.uk

scheme, Varaha. We build upon our previous presentation (Tiwari et al. 2023) and report an updated version of Varaha, a sampler highly efficient in small dimensions.

2 METHOD

Nested sampling is a robust tool to estimate gravitational wave posterior. Nested sampling converges to the peak of the likelihood distribution by iteratively drawing a series of contours of increasing likelihood. At the beginning, it draws a set of *live points*, n_{live} . At each cycle, it stores the live point with the lowest likelihood and replaces it with a new point drawn randomly from the prior. The new point is required to have a likelihood value greater than the smallest likelihood value of the live points. This scheme results in shrinkage of volume by an approximate factor of $\sim e^{-1/n_{\text{live}}}$. The new set of live points encompass a region of higher likelihood compared to the previous set. The stored points, along with their weight – the product of the average likelihood value and the volume enclosed between successive contours – constitute the *samples* drawn from the posterior distribution. Nested sampling suffers from two drawbacks, i) it has to cross-reference the likelihood values at each iteration making likelihood calculation impractical to parallelise over a large number of CPUs, and ii) a live point is replaced only after a point of higher likelihood has been obtained. This results in discarding a large number of points where likelihood is calculated. When estimating compact binary parameters from gravitational waves, most of the points where likelihood was calculated are often discarded ($\sim 99.9\%$).

Parallel Bilby improves the process parallelisation by independently advancing live points on multiple CPU nodes. On obtaining points higher in likelihood all the points are collected and new live points are defined (Smith et al. 2020a). Thus, Parallel Bilby can shrink the volume by a factor greater than $\sim e^{-1/n_{\text{live}}}$ at each iteration. However, Parallel Bilby is better suited for expensive likelihoods as the overhead cost of invoking parallelisation at each iteration may become high. The number of likelihood calculations also increases as not all the points accepted on different CPU nodes eventually get included as live points.

For general problems nested sampling provides an astute methodology to properly estimate the sampling density at each iteration. A possible way to improve the sampling efficiency would be to keep all the points and to explicitly calculate their sampling density. This approach is expected to become cumbersome with an increase in the number of parameters. However, in the context of compact binaries, often the number of parameters is not large. For example, there are 15 parameters for a precessing binary (8 and 7 if the sampling is broken into extrinsic and intrinsic parameters) (Ashton et al. 2019). The inclusion of calibration errors significantly increases the number of parameters (Abbott et al. 2016) but as none of the additional parameters are expected to be correlated with the binary parameters, these can be treated separately (Payne et al. 2020).

To explicitly calculate the sampling density we build a recipe based on a previous work (Tiwari et al. 2023). We review the previous work as follows. We begin by sprinkling the full parameter space with N points. On selecting n points with the largest likelihood values we carve a volume which is enclosed by the minimum likelihood value among all the selected points, \mathcal{L}_* . This volume, $V(\mathcal{L}_*)$ can be estimated using Monte Carlo (MC) integration,

$$V(\mathcal{L}_*) \approx \bar{V}(\mathcal{L}_*) = V_0 \frac{n}{N}, \quad \delta\bar{V} = \frac{\bar{V}}{\sqrt{n}}, \quad (1)$$

where V_0 is the full volume of the parameter space and $\delta\bar{V}(\mathcal{L}_*)$ is the

error on the estimated volume, $\bar{V}(\mathcal{L}_*)$. The structure of this volume is not known. But, on binning the full parameter space with bin size equal to $\delta\bar{V}(\mathcal{L}_*)$ and selecting the bins that include at least one of the selected points we reconstruct a volume (referred as *live volume* from now on). Live volume is expected to enclose most of the – if not all – *true* volume. We are focused on Gaussian likelihood (Abbott et al. 2016) when estimating GW posterior. For this likelihood, the distribution smoothly decays from a peak value. The error in the posterior probability is significantly smaller than the error in the volume – which is expected to be incurred away from the bulk probability in the lower-likelihood regions. That is, for the likelihood distribution $\mathcal{L}(d|\theta)$ defined on parameters θ and prior distribution $\pi(\theta)$, we can expect,

$$\int_{\mathcal{L} > \mathcal{L}_*} \mathcal{L}(d|\theta) \pi(\theta) d\theta \ll \int_{\mathcal{L} > \mathcal{L}_*} \pi(\theta) d\theta. \quad (2)$$

Thus, just sampling from the bins will in practice increase the number of data points with $\mathcal{L} > \mathcal{L}_*$ while ensuring that all the parameter space enclosed by the likelihood threshold \mathcal{L}_* has been sampled. From the second cycle onwards the procedure is repeated while only considering points with $\mathcal{L} > \mathcal{L}_*$ and discarding the rest. This is outlined pictorially in Fig. 1. The likelihood threshold, \mathcal{L}_* , is allowed to evolve until the probability mass discarded by the analysis reaches a pre-chosen threshold (Tiwari et al. 2023). The likelihood threshold is not decreased any further and the enclosed volume is repeatedly sampled until a desired number of posterior samples are collected. As the bins cover a volume that encloses almost all of the probability mass, keeping track of sampling density is not needed.

In the presented analysis we evolve the likelihood threshold to the peak of the likelihood distribution. This results in increased sampling efficiency as the bins now densely sample the high-likelihood regions of the likelihood distribution. However, we now need to explicitly calculate the sampling density of the sampled points. With N_j^i samples drawn from the j^{th} bin, in the i^{th} iteration/cycle, the sampling density for the k^{th} sample is

$$\rho_k = \sum_i \frac{N_j^i}{\delta\bar{V}^i} \Theta(j^i, k), \quad (3)$$

where $\delta\bar{V}^i$ is the estimated error in the MC volume at the i^{th} iteration/cycle. $\Theta(j^i, k)$ is one when the k^{th} sample overlaps with the j^{th} bin in the i^{th} cycle. Thus, Eq. 3 obtains the sampling density for a point by adding contributions from overlapping bins in all the cycles. For samples drawn at the current cycle, Eq. 3 needs to be calculated fully, however, for the samples drawn in previous cycles, the sampling density needs to be updated by the contributions coming from bins in the current cycle. That is for the current cycle i , any k^{th} sample drawn in a previous cycle will have an increase in its sampling density by,

$$\frac{N_j^i}{\delta\bar{V}^i} \Theta(j^i, k). \quad (4)$$

The samples don't carry equal weights because of different sampling densities. Rather, their weight is given by the inverse of the sampling density,

$$w_k = \frac{1}{\rho_k}. \quad (5)$$

The index k covers all the collected samples. Instead of choosing n points with the largest likelihood values, the analysis selects the next

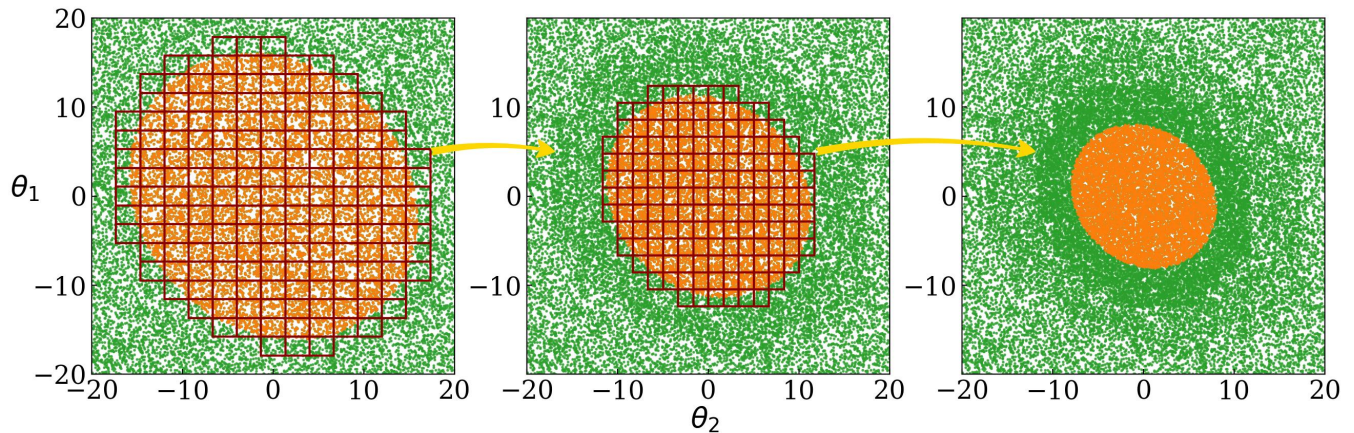


Figure 1. Sprinkling N points (green point) in a volume and selecting n points (orange points) with largest likelihood values carves a volume that is approximately $V(\mathcal{L}_*) \sim n/N$. The error associated with this volume is $\delta V(\mathcal{L}_*) \sim 1/\sqrt{n}$. Binning the parameter space with bin size equal to δV and selecting bins that enclose at least one of the selected points (red grid) ensures the maximum *true* volume not included by the selected bins is δV . For *Gaussian likelihoods*, error on volume always implies a significantly small error in probability mass enclosed by the likelihood threshold \mathcal{L}_* . Thus, only sampling from the bins at the next cycle ensures the parameter space enclosed by \mathcal{L}_* has been sufficiently sampled. The analysis keeps evolving until a stopping criterion is met.

likelihood threshold, \mathcal{L}_*^{i+1} , that shrinks the volume by a factor f . This new threshold will satisfy,

$$f = \frac{\sum_k w_k(\mathcal{L}_k > \mathcal{L}_*^{i+1})}{\sum_k w_k(\mathcal{L}_k > \mathcal{L}_*^i)}, \quad \bar{V}^{i+1} = f \bar{V}^i, \quad 0 < f < 1, \quad (6)$$

where the inequality in the brackets puts a condition on the sample to qualify for addition. The fractional error on the volume \bar{V}^{i+1} is

$$\frac{\delta \bar{V}^{i+1}}{\bar{V}^{i+1}} = f \sqrt{\frac{\text{var}(A)}{A^2} + \frac{\text{var}(B)}{B^2} - 2 \frac{\text{cov}(A, B)}{AB}}, \quad (7)$$

where A and B are numerator and denominator in the Eq. 6. Var and Cov stand for variance and covariance. The error is small for large f . For small values of f , only the first term in Eq. 7 contributes and the error reduces to,

$$\delta \bar{V}^{i+1} = \frac{\bar{V}^{i+1}}{\sqrt{n_{\text{eff}}^{i+1}}} \quad (8)$$

where n_{eff}^{i+1} is the effective prior-sample size enclosed by the likelihood threshold, \mathcal{L}_*^{i+1} (Martino et al. 2017; Tiwari 2018),

$$n_{\text{eff}}^{i+1} = \frac{\left(\sum_k w_k(\mathcal{L}_k > \mathcal{L}_*^{i+1})\right)^2}{\sum_k \left(w_k(\mathcal{L}_k > \mathcal{L}_*^{i+1})\right)^2}. \quad (9)$$

The value of the likelihood threshold increases with each cycle. The volume enclosed by the likelihood threshold, \mathcal{L}_*^i gradually decreases as the cycles proceed (for the full volume V_0 , the corresponding likelihood threshold is $-\infty$),

$$\bar{V}(\mathcal{L}_*^l) = V_0 f^l = V_0 \prod_{i=0}^{l-1} \frac{\sum_k w_k(\mathcal{L}_k > \mathcal{L}_*^{i+1})}{\sum_k w_k(\mathcal{L}_k > \mathcal{L}_*^i)} = V_0 \frac{\sum_k w_k(\mathcal{L}_k > \mathcal{L}_*^l)}{\sum_k w_k}. \quad (10)$$

In Eq.7 we have ignored the error in \bar{V}^i . To accommodate this error we shrink the volume by a fraction close to one but create bins with a size equal to the conservative estimate of the error in volume. This

is given in Eq. 8. Eq.6 suggests that accurate measurement of \mathcal{L}_*^{i+1} depends on $\sum_k w_k(\mathcal{L}_k > \mathcal{L}_*^i)$ and the error $\delta \bar{V}^{i+1}$ depends on n_{eff}^i .

The effective prior-sample size indicates how densely the space has been sampled. The reduced prior-sample size indicates how disparate the sampling densities are in the sampled space. If sampling is rigorous the two are expected to be proportional. We define a volume enclosed by a likelihood threshold sufficiently sampled by requiring them to be greater than some pre-chosen desired numbers. As we can only control $\delta \bar{V}^i$ in the analysis, the bins may not adequately sample the parameter space if there are features in the distribution that are smaller than this error. Thus, care must be taken when making the choices. For the examples presented in this article, we have chosen an effective prior-sample size greater than 10,000 which ensures a conservative estimate of the error on volume to be approximately 1%. But, as large errors are related to small values of f , we choose $f = 0.95$ to ensure that the error in reality is much smaller. We also require a reduced-sample size greater than 2,000. The reduced sample size indicates the number of independent samples enclosed by the likelihood threshold. This has semblance with the nested sampling where the number of independent samples enclosed by the likelihood threshold is the number of live points. Thus, our choice is the same as what is regularly used for the number of live points when using nested sampling in obtaining gravitational wave posterior (Smith et al. 2020b).

2.1 Stopping Criteria

The sampling weight when multiplied by the likelihood value gives the posterior distribution.

$$\mathbf{w}_k = w_k \mathcal{L}_k, \quad (11)$$

¹ Please note, $\sum_k w_k(\mathcal{L}_k > \mathcal{L}_*^i) / \max(w_k(\mathcal{L}_k > \mathcal{L}_*^i))$ is reduced prior-sample size, which informs the approximate number of equal weight samples one can obtain by performing rejection sampling on the reduced sampling weights, $w_k(\mathcal{L}_k > \mathcal{L}_*^i) / \max(w_k(\mathcal{L}_k > \mathcal{L}_*^i))$. Moreover, $n_{\text{eff}}^{i+1} \approx f n_{\text{eff}}^i$.

the effective posterior-sample size is given by²

$$n_{\text{eff}}^{\mathbf{w}} = \frac{(\sum_k \mathbf{w}_k)^2}{\sum_k (\mathbf{w}_k)^2}. \quad (12)$$

Evidence normalises the posterior probability distribution and is thus just the sum of these weights,

$$\mathcal{Z} = \sum_k \mathbf{w}_k. \quad (13)$$

Finally, the total probability enclosed by a likelihood threshold is,

$$\int_{\mathcal{L}(\theta) > \mathcal{L}_*} \mathcal{L}(d|\theta) \pi(\theta) d\theta \approx \bar{P}(\mathcal{L}_*) = \frac{\sum_k \mathbf{w}_k (\mathcal{L}_k > \mathcal{L}_*)}{\sum_k \mathbf{w}_k}. \quad (14)$$

The numerator is summed only for samples with a likelihood value greater than \mathcal{L}_* . Stopping criteria can be defined in several ways. Some examples when an analysis can be terminated include

- (i) a chosen number of effective samples have been collected,
- (ii) increase in marginal likelihood stagnates,
- (iii) the probability enclosed by a likelihood threshold becomes smaller than a prechosen value.

For the presented analysis we stop the analysis when $\bar{P} < 0.05$, i.e. the likelihood threshold encloses less than 5% probability.

2.2 Increase in Dimensionality

Varaha becomes increasingly inefficient with the increase in dimensionality. For a D dimensional space, if each dimension has the same number of bins, the number of bins in each dimension is $\sim (\delta \bar{V}(\mathcal{L}_*))^{(-1/D)}$. For larger dimensionality, the number of bins becomes smaller, resulting in the live volume becoming significantly bigger than the true volume. The efficiency gained due to storing all the points is gradually lost due to inefficient sampling of the parameter space. Fig. 2 shows the conversion percentage of the number of likelihood calculations to the posterior's effective sample size for Varaha and Dynesty (Speagle 2020). The chosen distribution is Rosenbrock (Rosenbrock 1960; Feroz & Skilling 2013) which is a challenging distribution to sample and is often used in optimisation problems. The efficiency gradually decreases with increased dimensionality.

Increasing dimensionality also increases the number of cycle analyses take to complete. This results in an increase in computation needed to calculate the sampling density for each sample. Fig. 3 shows the wall time for sampling the Rosenbrock distribution for different dimensionality. Each likelihood calculation takes a fraction of a millisecond, thus constituting a small fraction of the wall time.

Varaha takes less time than Dynesty to collect one posterior sample for the dimensionalities discussed above. However, in the context of sampling GW posteriors, the number of parameters for a precessing binary is 15. At this dimension, Varaha is inefficient and takes hundreds of millions of likelihood calculations to complete

² Equal weighted samples can be obtained by performing rejection sampling using the normalised weights $\mathbf{w}_k / \max(\mathbf{w}_k)$.

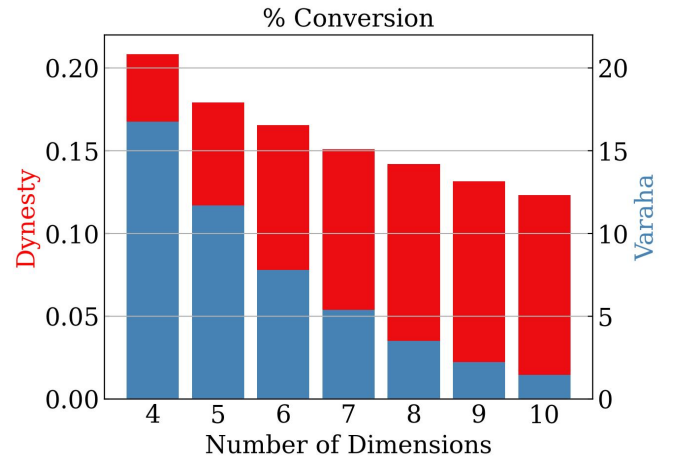


Figure 2. Percentage conversion of points at which likelihood was calculated to effective posterior sample size. The sampled distribution is Rosenbrock. The sampling uses the condition described in Section 3.

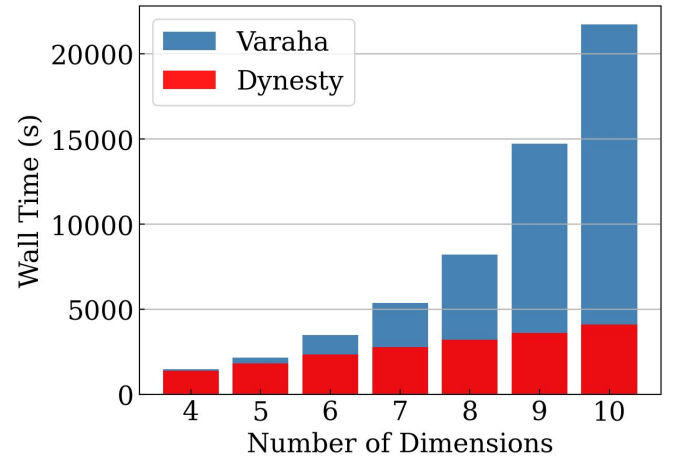


Figure 3. Sampling wall time for Varaha compared to Dynesty using one CPU. The sampled distribution is Rosenbrock. The sampling uses the condition described in Section 3. Likelihood calculations contribute only a small fraction of the total computation.

the sampling. Thus, in its current implementation, it is not a sampler of choice. However, it is possible to separately sample extrinsic and intrinsic parameters and break one large dimensional problem into two small dimensional ones (Pankow et al. 2015; Lange et al. 2018; Tiwari et al. 2023). Any dimensionality reduction improves Varaha's efficiency over Dynesty. Moreover, as the likelihood calculations are significantly more expensive, the wall time is dominated by likelihood calculations.

2.3 Parallelisation

An advantage of Varaha is to efficiently parallelise likelihood calculations over multiple processes. This is because of the significantly reduced number of likelihood cross-references in calculating the likelihood threshold compared to nested sampling. Fig. 4 shows the number of iterations/cycles used by Dynesty compared to Varaha. Varaha uses significantly less number of cycles. Each cycle calculates likeli-

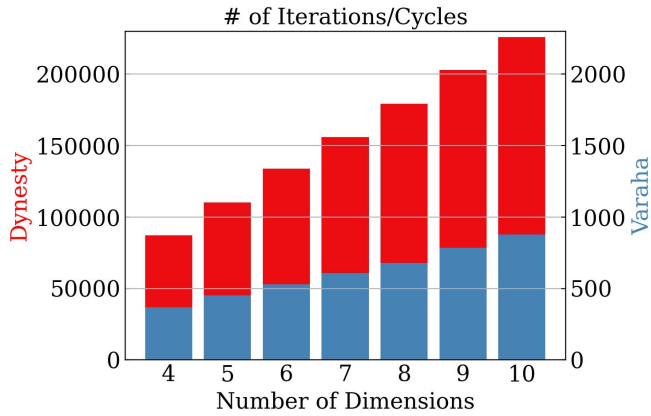


Figure 4. Number of iterations/cycles made by Dynesty compared to Varaha. The sampled distribution is Rosenbrock. The sampling uses the condition described at the end of subsection 2.1 and sets $N_w = 10,000$ and $n_w = 2,000$.

hood values over thousands of points which can be parallelised over several CPUs. The calculation of sampling density is also parallelisable. Different nodes can evaluate sampling density for different bins which can then be simply collected and added.

3 SAMPLING EXAMPLES

In this section, we discuss a few examples to showcase Varaha’s ability to sample challenging distributions. We also make comparisons with Nested Sampling. We have chosen seven dimensions for all the examples explicitly aiming for the relevant dimensionality when GW posteriors are obtained by separate sampling of extrinsic and intrinsic parameters.

For the examples discussed, Varaha shrank the volume by 95% in each cycle. The analysis proceeded to the next likelihood threshold only when the current likelihood threshold enclosed 2,000 reduced prior-samples and 10,000 effective prior-samples. We also sampled the distributions using Dynesty operated through the `BILBY` infrastructure (Ashton et al. 2019). We used the default settings provided by `BILBY` with some modifications to ensure reasonable convergence. Both samplers used a single CPU.

3.1 Bi-Modal Multivariate

We concoct a 7D bimodal distribution by combining two multivariate normal distributions. For the first normal we randomly chose means between -2 and -1. The covariance was drawn from the Wishart distribution. The scale was set to a diagonal matrix with elements randomly chosen between 1. and 1.5. The elements were further divided by 56. For the second normal we randomly chose means between 2 and 1. The covariance was drawn from the Wishart distribution. The scale was set to a diagonal matrix with elements randomly chosen between 1. and 1.5. The elements were further divided by 28. The mixing fraction was randomly chosen between 0.3 and 1.

For both Dynesty and Varaha we used a uniform prior between -20 and 20 for all the parameters. We used 2,000 live points for Dynesty. Dynesty collected 14,000 effective samples and estimated the log evidence to be -25.824 ± 0.091 . Varaha took 471 cycles. Varaha

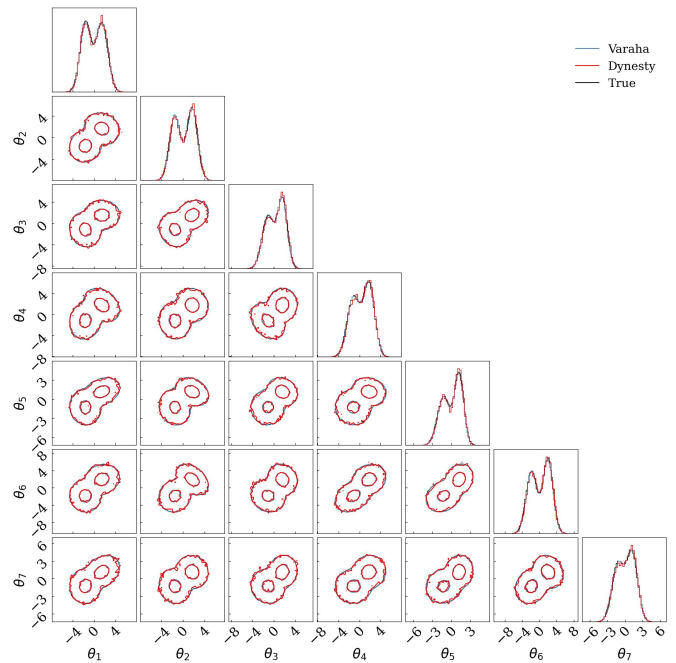


Figure 5. Percentage conversion of points at which likelihood was calculated to effective posterior-sample size. The sampled distribution is Bi-modal Gaussian

produced 6,41,300 effective samples and estimated log evidence to be -25.823 ± 0.015 . Evidence (marginal likelihood) was calculated using bootstrapping. Varaha was around forty times more efficient in converting points where likelihood was calculated to posterior samples. Varaha took double the wall time compared to Dynesty. Likelihood calculation was cheap, thus most of the time was consumed by overhead computation. The comparison for the sampled distribution is shown in Fig. 5.

3.2 Rosenbrock Distribution

Rosenbrock is a challenging distribution to sample because of high correlation between the parameters (Dittmann 2024).

For both Dynesty and Varaha we used a uniform prior between -5 and 5 for all the parameters. Dynesty took 1,56,000 iterations. to complete. We used 5,000 live points. Dynesty collected 41,000 effective posterior-samples and estimated the log evidence to be 28.993 ± 0.073 . Varaha took 586 cycles. Varaha collected 3,16,000 effective posterior-samples and estimated log evidence to be -29.05 ± 0.0267 . Evidence (marginal likelihood) was calculated using bootstrapping. Varaha was around forty times more efficient in converting points where likelihood was calculated to posterior samples. Varaha took double the wall time compared to Dynesty. Likelihood calculation was cheap, thus most of the time was consumed by overhead computation. The comparison for the sampled distribution is shown in Fig. 6.

Our previous version of the sampler is significantly less efficient—the percentage conversion of the points where likelihood was calculated to effective posterior-sample size is only 0.1%.

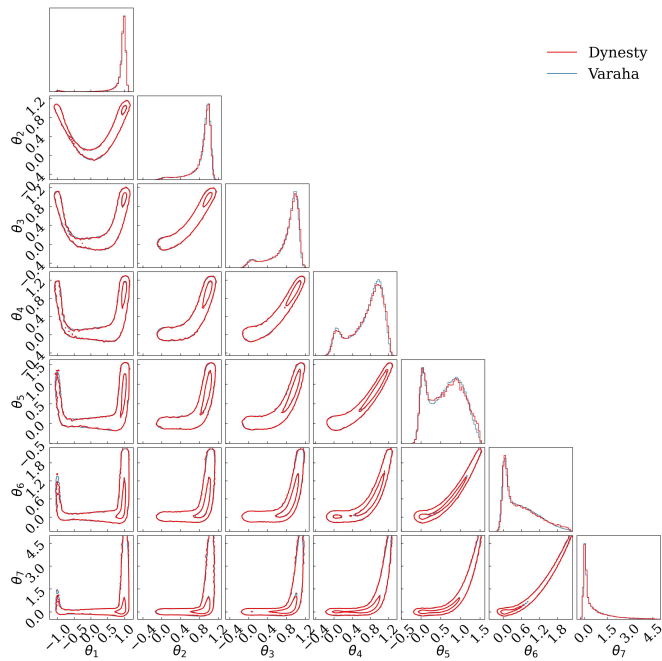


Figure 6. Percentage conversion of points at which likelihood was calculated to effective posterior-sample size. The sampled distribution is Rosenbrock. The sampling uses the condition described in Section 3.

Table 1. List of extrinsic parameters and the priors used. The GPS time $t_0 = 1126259462.411$.

Parameter	Uniform Prior	Description
α	$[0, 2\pi]$	Right ascension of the source
$\sin \delta$	$[-1, 1]$	Sine of declination of the source
d_L	$[0, 5 \times 10^3]$ Mpc	Luminosity distance of the source
$\cos \iota$	$[-1, 1]$	Cosine of the Inclination angle
ψ	$[0, \pi]$	Polarisation angle
ϕ_c	$[0, 2\pi]$	Coalescence phase
t_c	$t_0 + [0.1, -0.1]$	Coalescence time in the reference detector

3.3 Extrinsic Parameters for GW150914

We sampled the extrinsic parameters listed in Table 1 for the first GW signal GW150914 (Abbott et al. 2016). We used an aligned spin model IMRPHENOMD (Husa et al. 2016; Khan et al. 2016). This model ignores the components of the spins in the orbital plane of the binary leaving only the component masses and the component of spins aligned with orbital angular momentum as the only intrinsic parameters. For the component masses, we fixed, $m_1 = 36.80M_\odot$ and $m_2 = 31.96$, and the aligned spin components are fixed to $s_{1z} = -0.623$, $s_{2z} = 0.466$. We picked these values from a full sampling run separately performed using Dynesty. These choices correspond to the maximum likelihood value for that run.

We used 2,000 live points for Dynesty. Dynesty took 51,300 iterations to complete and collected 13,000 effective samples. Varaha took 1270 cycles to complete and collected 3,20,000 effective samples. Varaha was around twenty times more efficient in converting points where likelihood was calculated to posterior samples. Fig. 7 shows the sampled extrinsic parameter.

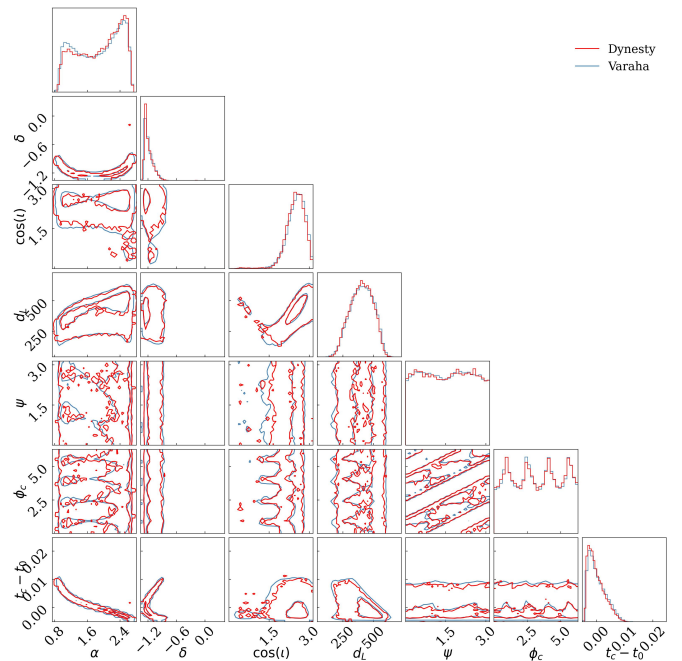


Figure 7. The sampled extrinsic dimensional extrinsic parameter space detailed in Table 1. The mean coalescence time is $t_0 = 1126259462.411$.

4 CONCLUSIONS

In this article, we presented a novel sampler that is significantly more efficient than Nested sampling for small dimensions (≤ 10). We built on a previous work and showed that in small dimensions it is possible to explicitly calculate the sampling density of all the sampled points. This sampling density along with the likelihood values constitutes the posterior distribution. Our sampler, Varaha, does not discard any points making it more efficient than nested sampling, but, as it becomes increasingly inefficient with increased dimensionality it is not a sampler of choice to sample the full parameter space of compact binaries. However, if the sampling is separated into parameters that are observer-dependent and parameters that are intrinsic to the binary we expect Varaha to be a sampler of choice. Not only it is efficient, but it is embarrassingly parallel, and as it retains all the samples, posterior corresponding to different priors can be efficiently obtained by re-weighting the sampling density. The presented version of Varaha is significantly more efficient than the previous version (Tiwari et al. 2023) which is better suited for cheaper likelihoods (e.g. when marginalising over extrinsic parameters). The new version comes with an added cost of estimating the sampling density but this cost constitutes only a small fraction of the total computational cost for more expensive likelihoods (e.g. when sampling intrinsic parameters using marginalised likelihoods which can take from a fraction of a second to a few seconds). The presented sampler is lightweight requiring less than four hundred lines of code.

ACKNOWLEDGEMENTS

Sincere thanks to Lalit Pathak for LIGO's Publications & Presentations review, to Alberto Vecchio, Patricia Schmidt and Stephen Fairhurst for helpful guidance on this project, and to Charlie Hoy for providing Varaha's interface for Bilby. This work was conducted on Cardiff University's HAWK HPC.

This material is based upon work supported by NSF's LIGO Laboratory which is a major facility fully funded by the National Science Foundation.

DATA AVAILABILITY

The examples and required code are available on [GitHub](#).

REFERENCES

- Abbott B. P., et al., 2016, *Phys. Rev. Lett.*, 116, 241102
- Abbott R., et al., 2020, *Living Reviews in Relativity*, 23, 3
- Abbott R., Abbott T. D., Acernese F., et al., 2021a, *arXiv e-prints*, p. [arXiv:2108.01045](#)
- Abbott R., Abbott T. D., Acernese F., et al., 2021b, *arXiv e-prints*, p. [arXiv:2111.03606](#)
- Adamcewicz C., Lasky P. D., Thrane E., 2023, *ApJ*, 958, 13
- Ashton G., et al., 2019, *The Astrophysical Journal Supplement Series*, 241, 27
- Callister T. A., Farr W. M., 2024, *Physical Review X*, 14, 021005
- Dax M., Green S. R., Gair J., Macke J. H., Buonanno A., Schölkopf B., 2021, *Phys. Rev. Lett.*, 127, 241103
- Dittmann A. J., 2024, <https://api.semanticscholar.org/CorpusID:269430717>
- Fairhurst S., Hoy C., Green R., Mills C., Usman S. A., 2023, *Phys. Rev. D*, 108, 082006
- Farah A. M., Edelman B., Zevin M., Fishbach M., María Ezquiaga J., Farr B., Holz D. E., 2023, *ApJ*, 955, 107
- Feroz F., Skilling J., 2013, *AIP Conference Proceedings*, 1553, 106
- Gabbard H., Messenger C., Heng I. S., Tonolini F., Murray-Smith R., 2022, *Nature Physics*, 18, 112
- Gupta I., 2024, *arXiv e-prints*, p. [arXiv:2402.07075](#)
- Heinzel J., Biscoveanu S., Vitale S., 2023, *arXiv e-prints*, p. [arXiv:2312.00993](#)
- Husa S., Khan S., Hannam M., Pürrer M., Ohme F., Forteza X. J., Bohé A., 2016, *Phys. Rev. D*, 93, 044006
- Khan S., et al., 2016, *Phys. Rev. D*, 93
- Lange J., O'Shaughnessy R., Rizzo M., 2018, *arXiv e-prints*, p. [arXiv:1805.10457](#)
- Leyde K., Green S. R., Toubiana A., Gair J., 2024, *Phys. Rev. D*, 109, 064056
- Magaña Hernandez I., Ray A., 2024, *arXiv e-prints*, p. [arXiv:2404.02522](#)
- Martino L., Victor E., Carlos S., 2017, *Signal Processing-Elsevier*, pp 386–401
- Morisaki S., 2021, *Phys. Rev. D*, 104, 044062
- Morisaki S., Raymond V., 2020, *Phys. Rev. D*, 102, 104020
- Morisaki S., Smith R., Tsukada L., Sachdev S., Stevenson S., Talbot C., Zimmerman A., 2023, *Phys. Rev. D*, 108, 123040
- Morrás G., Nuño Siles J. F., García-Bellido J., 2023, *Phys. Rev. D*, 108, 123025
- Narola H., Janquart J., Meijer Q., Haris K., Van Den Broeck C., 2023, *arXiv e-prints*, p. [arXiv:2308.12140](#)
- Pankow C., Brady P., Ochsner E., O'Shaughnessy R., 2015, *Phys. Rev. D*, 92, 023002
- Pathak L., Reza A., Sengupta A. S., 2023, *Phys. Rev. D*, 108, 064055
- Pathak L., Munishwar S., Reza A., Sengupta A. S., 2024, *Phys. Rev. D*, 109, 024053
- Payne E., Talbot C., Lasky P. D., Thrane E., Kissel J. S., 2020, *Phys. Rev. D*, 102, 122004
- Payne E., Kremer K., Zevin M., 2024, *ApJ*, 966, L16
- Pratten G., et al., 2021, *Phys. Rev. D*, 103, 104056
- Ray A., Hernandez I. M., Mohite S., Creighton J., Kapadia S., 2023, *ApJ*, 957, 37
- Rinaldi S., Del Pozzo W., Mapelli M., Lorenzo-Medina A., Dent T., 2024, *A&A*, 684, A204
- Rosenbrock H. H., 1960, *The Computer Journal*, 3, 175

- Roulet J., Mushkin J., Wadekar D., Venumadhav T., Zackay B., Zaldarriaga M., 2024, *arXiv e-prints*, p. [arXiv:2404.02435](#)
- Sadiq J., Dent T., Gieles M., 2024, *ApJ*, 960, 65
- Smith R. J. E., Ashton G., Vajpeyi A., Talbot C., 2020a, *MNRAS*, 498, 4492
- Smith R. J. E., Ashton G., Vajpeyi A., Talbot C., 2020b, *Mon. Not. Roy. Astron. Soc.*, 498, 4492
- Speagle J. S., 2020, *Mon. Not. Roy. Astron. Soc.*, 493, 3132
- The LIGO-Virgo-KAGRA (LVK) Collaboration 2023, *arXiv e-prints*, p. [arXiv:2304.08393](#)
- Tiwari V., 2018, *Classical and Quantum Gravity*, 35, 145009
- Tiwari V., Hoy C., Fairhurst S., MacLeod D., 2023, *Phys. Rev. D*, 108, 023001
- Williams M. J., Veitch J., Messenger C., 2021, *Phys. Rev. D*, 103, 103006
- Wong K. W. K., Isi M., Edwards T. D. P., 2023, *ApJ*, 958, 129

APPENDIX A: FILLING THE BINS

The choice of bin size and the number of samples drawn from bins substantially impact the evolution of the analysis. The number of bins in each dimension results in each hyper-cube occupying a volume in the parameter space. The requirement is to have this volume close to the error in volume. We did not make significant progress in optimising these elements. The analysis draws the number of bins in each dimension using the following ad hoc prescription,

$$B_j^i = B 2^{U(-1,1)} \quad \text{or} \quad \mathcal{N}(\mu = B, \sigma = \sqrt{B}), \quad i = \text{fixed}, j = 1 \cdots D \quad (\text{A1})$$

where $U(-1, 1)$ is a uniform draw between -1 and 1, \mathcal{N} is the normal distribution and $B = (\delta\bar{V}(\mathcal{L}_*^i))^{(-1/D)}$. One draw of D bins is not necessarily expected to have a hypercube volume close to $\delta\bar{V}(\mathcal{L}_*^i)$. Thus, we make several thousands of draws and choose the combination that has hypercube volume closest to $\delta\bar{V}(\mathcal{L}_*^i)$. Moreover, we switch between two prescriptions separated by the or condition in Eq. A1 depending on the cycle number being odd or even.

At a cycle, the number of samples needs to be increased such that shrink criteria defined in 2 is met. The parameter space is binned and bins that contain at least one sample with a likelihood threshold greater than \mathcal{L}_*^i are selected. The number of samples in bins is adjusted such that the summed sampling density in the bins is approximately uniform. The number of samples to be drawn from each bin is

$$N_j^i \propto B_j^i - \max(B_j^i), \quad B_j^i = \sum_k \rho_k(\mathcal{L}_k > \mathcal{L}_*^i) \Theta(j, k), \quad (\text{A2})$$

where the summed density in a bin, B_j^i is the sum of the sampling density of all the samples that cross the likelihood threshold \mathcal{L}_*^i and overlap with the j^{th} bin.

Each cycle approximately shrinks the volume by a factor f . This approximately implies that the number of samples enclosed by the new likelihood threshold is also f times the number of samples enclosed by the old likelihood threshold. Thus, the total number of samples that need to be compensated is $1 - f$ times the total number of samples. As not all samples drawn from bins are going to cross the likelihood threshold this needs to be divided by the acceptance fraction (ratio of number of samples that cross the likelihood threshold and the total number of samples drawn from the bins). Starting at the first cycle where almost all the points sampled from the parameter space cross the likelihood threshold, the acceptance fraction reduces as likelihood increases.

APPENDIX B: SAMPLING DENSITY CALCULATION

The sampling density calculation requires adding contributions from all the bins sampled in all the cycles. This has to be done for each sample. Each cycle shrinks the volume and proceeds to sample higher likelihood regions in the parameter space. Thus, removing the non-contributing samples and bins from earlier cycles speeds up the calculation of the sampling density. The analysis keeps all the samples that are enclosed by a volume twice the volume of the current cycle. That is for the current cycle i , any samples with a likelihood value smaller than $\mathcal{L}_*^{\text{keep}}$ are removed. $\mathcal{L}_*^{\text{keep}}$ is chosen, such that

$$\frac{\bar{V}^{\text{keep}}}{\bar{V}^i} > 2. \quad (\text{B1})$$

With increase in \mathcal{L}_*^i , there is increase in $\mathcal{L}_*^{\text{keep}}$. To avoid removing samples meaningfully contributing to the posterior the analysis does not increase $\mathcal{L}_*^{\text{keep}}$ if the following condition is met

$$\frac{\sum_k \mathbf{w}_k (\mathcal{L}_k > \mathcal{L}_*^i)}{\sum_k \mathbf{w}_k (\mathcal{L}_k > \mathcal{L}_*^{\text{keep}})} < 0.999; \quad (\text{B2})$$

the analysis stores all the samples enclosed by a volume that is double the volume that encloses 99.9% posterior probability mass.

Varaha creates and samples from bins at each likelihood threshold, \mathcal{L}_*^i . Bins created at a volume 32 times bigger than \bar{V}^{keep} are removed. This also requires the removal of samples drawn from these bins (these samples will have a likelihood greater than $\mathcal{L}_*^{\text{keep}}$). Moreover, the contribution to the sampling density for any samples overlapping with the removed bins also needs to be subtracted.

This paper has been typeset from a $\text{\TeX}/\text{\LaTeX}$ file prepared by the author.